Magnetic scattering effects in two-band superconductor: the ferromagnetic dopants in MgB_2

2010 J. Phys.: Condens. Matter 22 135701

(http://iopscience.iop.org/0953-8984/22/13/135701)

J. Phys.: Condens. Matter **22** (2010) 135701 (8pp) doi:10.1088/0953-8984/22/13/135701

Magnetic scattering effects in two-band superconductor: the ferromagnetic dopants in MgB_2

W X Li[1,2], R Zeng[1], C K Poh[1], Y Li[2] and S X Dou[1,3]

[1] Institute for Superconducting and Electronic Materials, University of Wollongong, Wollongong, NSW 2522, Australia
[2] School of Materials Science and Engineering, Shanghai University, 149 Yanchang Road, Shanghai 200072, People's Republic of China

E-mail: shi@uow.edu.au

Received 28 September 2009, in final form 19 February 2010
Published 12 March 2010
Online at stacks.iop.org/JPhysCM/22/135701

Abstract

This paper demonstrates the magnetic scattering effects on the electron–phonon interaction in two-band superconductors based on the transition-metal-doped MgB_2 to clarify the effects of magnetic dopants on multi-band superconductivity. The phonon properties of polycrystalline $Mg_{1-x}M_xB_2$ (M = Fe, Ni and Co), with x up to 0.05, were studied, with the investigation based on the normal state Raman spectra, especially the variation of the E_{2g} mode. The magnetic scattering effect of Fe is much weaker than that of Mn in MgB_2, while it is stronger than that of Ni. The weak magnetic scattering effects are responsible for the superconducting behaviors of $Mg_{1-x}Fe_xB_2$ and $Mg_{1-x}Ni_xB_2$. Co shows almost no magnetic scattering effects on the superconductivity, while the depression of the critical temperature, T_c, in $Mg_{1-x}Co_xB_2$ is attributed to the phonon behavior and is independent of the ferromagnetic nature of cobalt.

(Some figures in this article are in colour only in the electronic version)

1. Introduction

Magnetic impurities in conventional phonon-mediated single-band superconductors induce pair-breaking effects via spin-flip scattering, while the pair-breaking mostly results from inter- and intra-band scattering from both magnetic and non-magnetic impurities in the unconventional multi-band superconductors. The exchange interaction between conduction electrons and the magnetic dopant ions does not depend solely on the exact nature of the impurity. MgB_2 is a two-gap superconductor characterized by a two-dimensional σ band and a three-dimensional π band [1]. Its critical transition temperature, T_c, mainly originates from the σ band and depends on the electron (hole) doping intensity and the inter-band scattering. The intense depression in T_c of $Mg_{1-x}Mn_xB_2$ is due to the increased magnetic pair-breaking resulting from spin-flip scattering in the σ bands, with possible contributions from the π–π or σ–π channels [2–4]. The Mn doping effects on MgB_2 are in agreement with the Abrikosov–Gorkov pair-breaking theory [4, 5]. The scattering behavior of Fe [6] is different both from that of the magnetic impurity Mn and from those of the non-magnetic impurities Al [7] and C [8]. Although the phonon contribution is predicted to be responsible for the reduction in T_c of $Mg_{1-x}Fe_xB_2$, the explanation for the particular effects of Fe doping on the superconductivity of MgB_2, such as the inconsistent variation in the electronic behavior and superconducting properties, is still unclear [6, 9].

Owing to the simple hexagonal structure with space group $P6/mmm$, four optical modes at the Γ-point of the Brillouin zone are predicted for MgB_2: a silent B_{1g} mode (at 87.1 meV, ∼700 cm^{-1}), the E_{2g} Raman mode (at 74.5 meV, ∼600 cm^{-1}) and the infrared-active E_{1u} (at 40.7 meV, ∼330 cm^{-1}) and A_{2u} (at 49.8 meV, ∼400 cm^{-1}) modes. The detectable phonon parameters in measurements of the spectral features are the phonon frequency, the linewidth (full width at half-maximum, FWHM) and the intensity, which can all be affected by the electron–phonon coupling (EPC). Frequency shifts and

[3] Author to whom any correspondence should be addressed.

linewidth variations in particular can represent a change in the phonon characteristics. The superconducting energy gaps and changes in the phonon lineshapes of MgB_2 below T_c have been studied by the Raman response because the pairing gaps on the 2D σ bands and the 3D π bands can be observed directly, due to the symmetry dependence of the Raman spectra [10]. The strength and frequency dependence of the EPC is determined by both the bare phonon density of states (PDOS), $F(\omega)$, and the electron–phonon spectral density, $\alpha^2(\omega)F(\omega)$, where α is the absorption coefficient. During exploration of the superconductivity in MgB_2, Raman response measurements have contributed greatly to the understanding of the superconducting mechanism. This is because the E_{2g} mode is Raman-active and strongly coupled to the electronic conduction σ bands. The significant broadening of this Raman peak arises mainly from the exceptionally strong EPC of the E_{2g} mode in the partially occupied planar boron σ bands near the Fermi surface [11].

In this work, the electrical resistivity and Raman spectrum were measured for $Mg_{1-x}Fe_xB_2$, with x up to 0.05, to study the Fe doping effects on the electron–phonon coupling. Co and Ni doping effects are also explored to compare their influences on the superconductivity of MgB_2 with those of Fe. The magnetic scattering effects on superconductive behavior are discussed, based on the electron–phonon coupling of the E_{2g} mode. The results are compared with the theoretical predictions to explore the effects of the ferromagnetic dopants on the superconductivity of MgB_2.

2. Experiments

Polycrystalline Fe-, Co- and Ni-doped MgB_2 samples with nominal compositions of $Mg_{1-x}M_xB_2$ (M = Fe, Co, Ni; x = 0, 0.005, 0.01, 0.02, 0.03 and 0.05) were synthesized by *in situ* solid state reaction. The starting materials were mixed together in the appropriate stoichiometric ratio and pressed into pellets 10 mm in diameter and about 5 mm in thickness, under a pressure of ∼600 MPa. Then the samples were sintered in a tube furnace at 800 °C for 10 h under high-purity argon gas flow, at a heating rate of 5 °C min^{-1}, and furnace-cooled to room temperature. The crystal structures were characterized by x-ray diffraction (XRD; D/ max -2200). The temperature-dependent electrical resistivity, $\rho(T)$, was measured over the temperature range from 4.2 to 300 K using a Physical Properties Measurement System (PPMS; Quantum Design). The T_c values are defined by the onset point from the $\rho(T)$ curves. The Raman scattering was measured by a confocal laser Raman spectrometer (Renishaw inVia plus) with a 100× microscope. The 514.5 nm line of an Ar^+ laser was used for excitation, with the laser power maintained at about 20 mW.

3. Results and discussion

XRD patterns of $Mg_{1-x}Fe_xB_2$, $Mg_{1-x}Co_xB_2$ and $Mg_{1-x}Ni_xB_2$ are shown in figure 1. The main phases are MgB_2 in all the samples with a small amount of MgO. FeO and NiO are the main impurity phases in high doping level $Mg_{1-x}Fe_xB_2$ and $Mg_{1-x}Ni_xB_2$, respectively. Co_3O_4, CoMg and residual Co can be found in the high doping level $Mg_{1-x}Co_xB_2$. Furthermore, traces of MgB_7 are found in $Mg_{1-x}Ni_xB_2$ and $Mg_{1-x}Co_xB_2$ for x = 0.03 and 0.05 due to the Mg insufficiency caused by the formation of the NiMg and CoMg alloys. The DC susceptibility measurements show an obvious magnetic background for the doped samples due to the unreacted dopants and resultants of subsidiary reactions. The magnetic moments of the second phases are much higher than those of diamagnetic MgB_2, 10^{-6} emu mol^{-1} at 300 K [12]. Then the transport measurement is employed to determine the T_c values to avoid the influence of the strong magnetic moment.

The resistivity dependence on temperature $\rho(T)$ was measured to confirm the T_c values, in order to avoid the effects of magnetic impurities in susceptibility measurements. The measured $\rho(T)$ data are shown as solid squares (■) in figure 2, while the orange lines are merely guides to the eyes for the trends in the normal state resistivity. The $\rho(T)$ behaviors are similar to those of Mn-, C- or Al-doped MgB_2 and there are no signs of spin-flip effects. The most obvious results of ferromagnetic dopant addition are the depressed T_c and the increased normal state resistivity values. The T_c dependence on the Fe, Co and Ni doping levels in MgB_2 deduced from the $\rho(T)$ curves is shown in figure 3. The T_c of $Mg_{1-x}Fe_xB_2$ shows a steep decrease, with a slope of $dT_c/dx \approx -170$, which is almost three times more rapid than the equivalent with Co doping, −65, and two times more rapid than that with Ni doping, −95. However, the T_c degradation of $Mg_{1-x}Fe_xB_2$ with increasing x is much gentler than that of Mn-doped MgB_2 [3, 4]. The values of the residual resistivity, ρ_0, increase with increasing doping level for all samples in this research, as shown in figure 4. Although the multi-band theory indicates that the T_c depends directly on ρ_0, it has been proved that this relationship does not exist in MgB_2 [13]. This is because ρ_0 values are determined by both intrinsic and intergrain contributions, depending on the different processing methods and raw materials. Despite the linear dependence of T_c on ρ_0 that exists in individual Fe-, Co- or Ni-doped MgB_2 samples, these linear plots have different gradients, as shown in the inset of figure 4, and such a discrepancy is in stark contrast with the prediction. The impurity scattering between the σ and the π bands is exceptionally small due to the particular electronic structure of MgB_2 [14]. Thus, the large variation in the residual resistivity primarily reflects a large variation of the scattering rate inside the σ and π bands. The scattering ratio in the two types of bands is hard to extract within a multi-band model in samples with poor intergrain connectivity.

Theoretically, the effect of magnetic impurities on the normal and superconductive properties of a multi-band s-wave superconductor [15–18] can be estimated by direct solution of the two-band Eliashberg equations [8, 14, 19–24]. The numerical results show that the magnetic impurities are responsible for the unusual behavior of the superconducting gaps and the penetration lengths as a function of temperature [15]. The possibility is examined that the presence of a negative induced gap raises the critical temperature. Singh *et al* [25] have calculated the electronic structure of the three-dimensional transition-metal–MgB_2 alloys, $Mg_{0.97}TM_{0.03}B_2$,

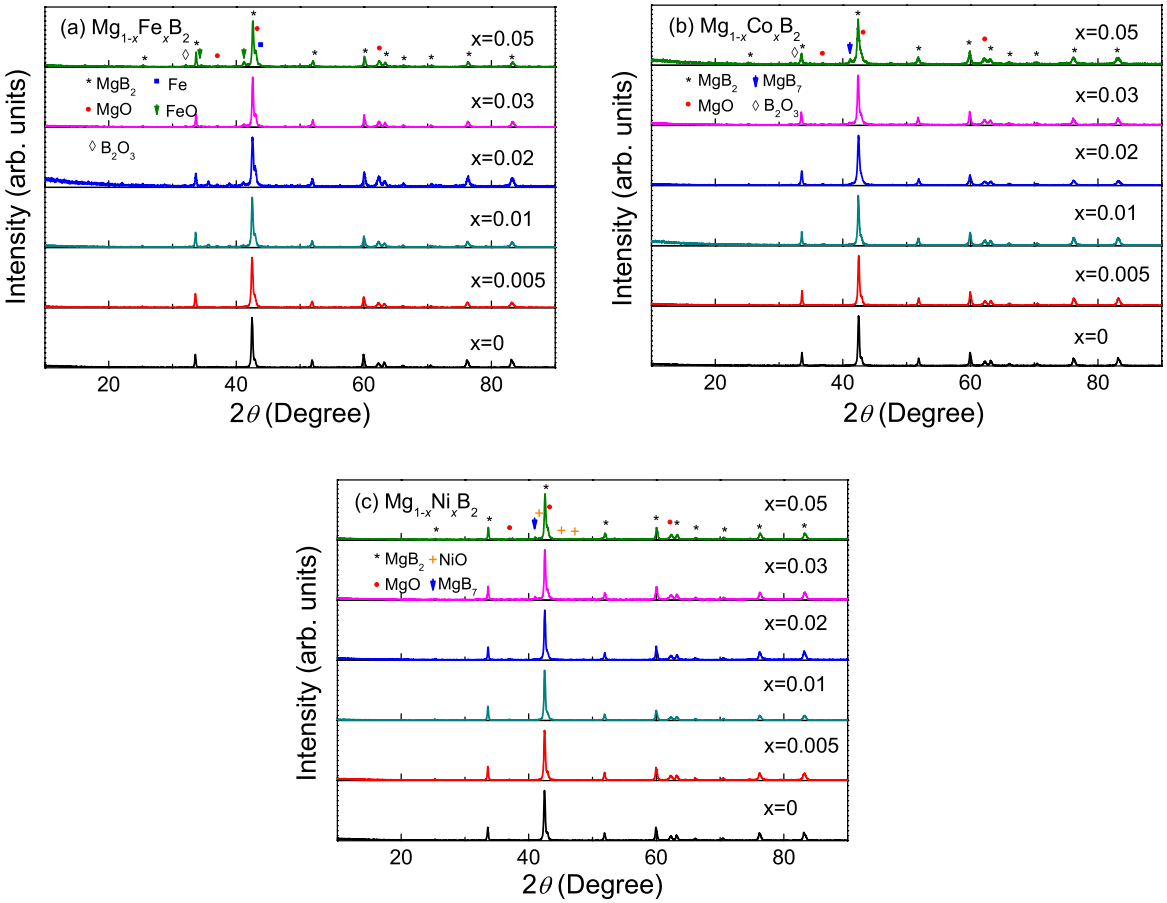

Figure 1. XRD patterns of $Mg_{1-x}Fe_xB_2$ (a), $Mg_{1-x}Co_xB_2$ (b) and $Mg_{1-x}Ni_xB_2$ (c).

using the Korringa–Kohn–Rostoker coherent-potential approximation method in the atomic-sphere approximation with TM = Sc, T, V, Cr, Mn, Fe, Co, Ni, Cu and Zn. The spin-polarized calculations show that V-, Cr-, Mn-, Fe- and Co-doped MgB_2 are magnetic, with the magnetic moments of $Mg_{0.97}Cr_{0.03}B_2$ and $Mg_{0.97}Mn_{0.03}B_2$ in particular as strong as 2.43 and 2.87 μ_B/atom, where μ_B is the Bohr magneton, whereas it is very weak for $Mg_{0.97}Co_{0.03}B_2$, only 0.01 μ_B/atom. The electron–phonon coupling constant, λ, and T_c are calculated using the Gaspari–Gyorffy formalism and the Allen–Dynes equation, respectively. $Mg_{0.97}Zn_{0.03}B_2$ is found to show the highest T_c value, which is in agreement with the experimental results. The variation of T_c, in terms of the DOS and the spectral function along the Γ to A direction in the Brillouin zone, is the result of the interplay between the total DOS at the Fermi energy and the creation/removal of states along the Γ to A direction. The controversial point of the research is the use of the Allen–Dynes formula for the calculation of T_c values because this formula is not suitable for the system with magnetic impurities [22]. The calculated low T_c of $Mg_{1-x}Co_xB_2$ contradicts the experimental results. The calculation results of Joseph *et al* [2] show that the Mn forms a local magnetic moment of 1.84 μ_B/atom in $Mg_{0.95}Mn_{0.05}B_2$, which is much weaker than the results of Singh *et al*. In contrast, the Fe impurities in $Mg_{0.95}Fe_{0.05}B_2$ tend to remain feebly magnetic with a local magnetic moment of 0.04 μ_B/atom. Gahtori *et al* have found that the electrical resistivity, thermal conductivity and Seebeck coefficient are free of the magnetism of the Fe in $Mg_{1-x}Fe_xB_2$. The weak effects of the magnetic moment on superconductivity are difficult to be observed directly. Considering the dominant effect of the E_{2g} mode on the superconductivity of MgB_2, the Fe, Co and Ni doping effects on the E_{2g} mode need to be measured and discussed systematically to explain the T_c dependence on the Fe, Co and Ni doping levels. The Raman scattering measurement was employed to detect the electron–phonon coupling behaviors in $Mg_{1-x}Fe_xB_2$, $Mg_{1-x}Co_xB_2$ and $Mg_{1-x}Ni_xB_2$.

The Raman spectra of all the samples can be fitted with three broad peaks [26], as shown in figure 5. The broad peaks centered at ~580 cm^{-1} are the reflections of the Raman-active E_{2g} mode, whereas the peaks centered at ~400 and ~780 cm^{-1} are attributed to the strong PDOS coming from the violation of Raman selection rules induced by disorder. As a phonon-mediated superconductor [27], the properties of the E_{2g} mode are directly related to the superconductivity of MgB_2. The fitting parameters of the E_{2g} modes show very different behavior in $Mg_{1-x}Fe_xB_2$, $Mg_{1-x}Co_xB_2$ and $Mg_{1-x}Ni_xB_2$, as shown in figures 6 and 7. The Raman shifts of the E_{2g} mode in $Mg_{1-x}Fe_xB_2$ increase quickly with doping level, while the values of $Mg_{1-x}Ni_xB_2$ are inversely proportional to the doping level. However, Co substitution does not obviously change

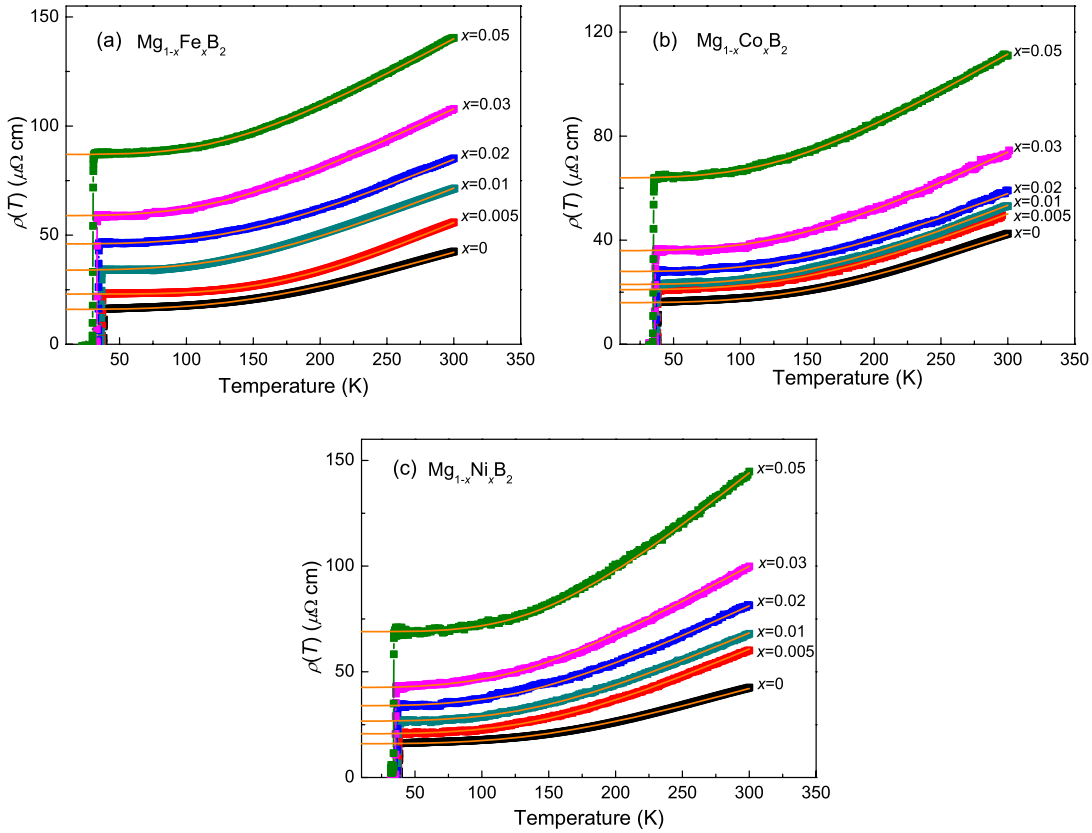

Figure 2. Measured $\rho(T)$ curves of $Mg_{1-x}Fe_xB_2$ (a), $Mg_{1-x}Co_xB_2$ (b) and $Mg_{1-x}Ni_xB_2$ (c) in the range of 20–300 K. The solid squares (■) are experimental results and the orange solid lines are guides to the eyes.

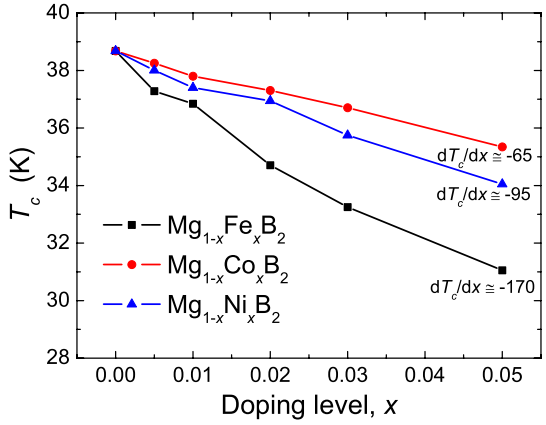

Figure 3. Measured critical superconducting transition temperature, T_c, for $Mg_{1-x}Fe_xB_2$, $Mg_{1-x}Co_xB_2$ and $Mg_{1-x}Ni_xB_2$.

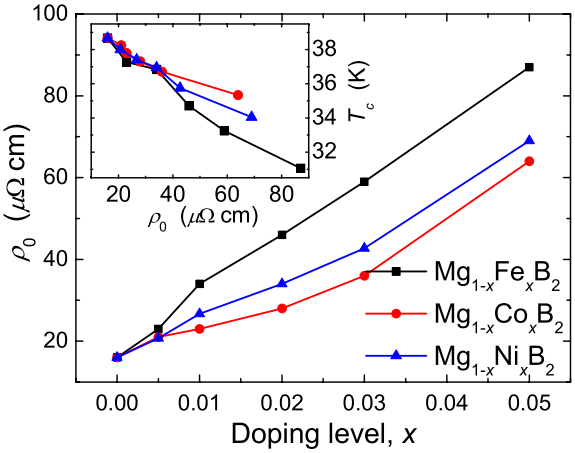

Figure 4. Residual resistivity, ρ_0, for $Mg_{1-x}Fe_xB_2$, $Mg_{1-x}Co_xB_2$ and $Mg_{1-x}Ni_xB_2$. The inset shows the T_c dependence on ρ_0.

the frequency of the E_{2g} mode in MgB_2. On comparing the Raman shifts of $Mg_{1-x}Fe_xB_2$, $Mg_{1-x}Co_xB_2$ and $Mg_{1-x}Ni_xB_2$, no clear clue can be found to the T_c properties because the electron–phonon coupling strength of the E_{2g} mode depends on both the frequency and the FWHM. So far as the contribution of the E_{2g} mode to the superconductivity is concerned, the linewidth of the E_{2g} mode reveals the intensity of the electron–E_{2g} coupling. The linewidths of the E_{2g} mode for Fe- and Ni-doped MgB_2 remain almost stable with increasing doping level, while those for Co-doped MgB_2 decrease, as shown in figure 7.

Based on the frequency and linewidth of the E_{2g} mode, direct evaluation of the contribution of the E_{2g} mode to the EPC is possible [28]. The dependence of the electron–E_{2g} constant on the phonon frequency and linewidth is given by the Allen equation [29]:

$$\lambda_{e-E_{2g}} = \frac{\Gamma_2}{2\pi N(0)\omega_2^2}, \quad (1)$$

where $\lambda_{e-E_{2g}}$ is the electron–E_{2g} coupling constant and $N(0)$ is the number of DOS (states/eV cell spin) on the Fermi

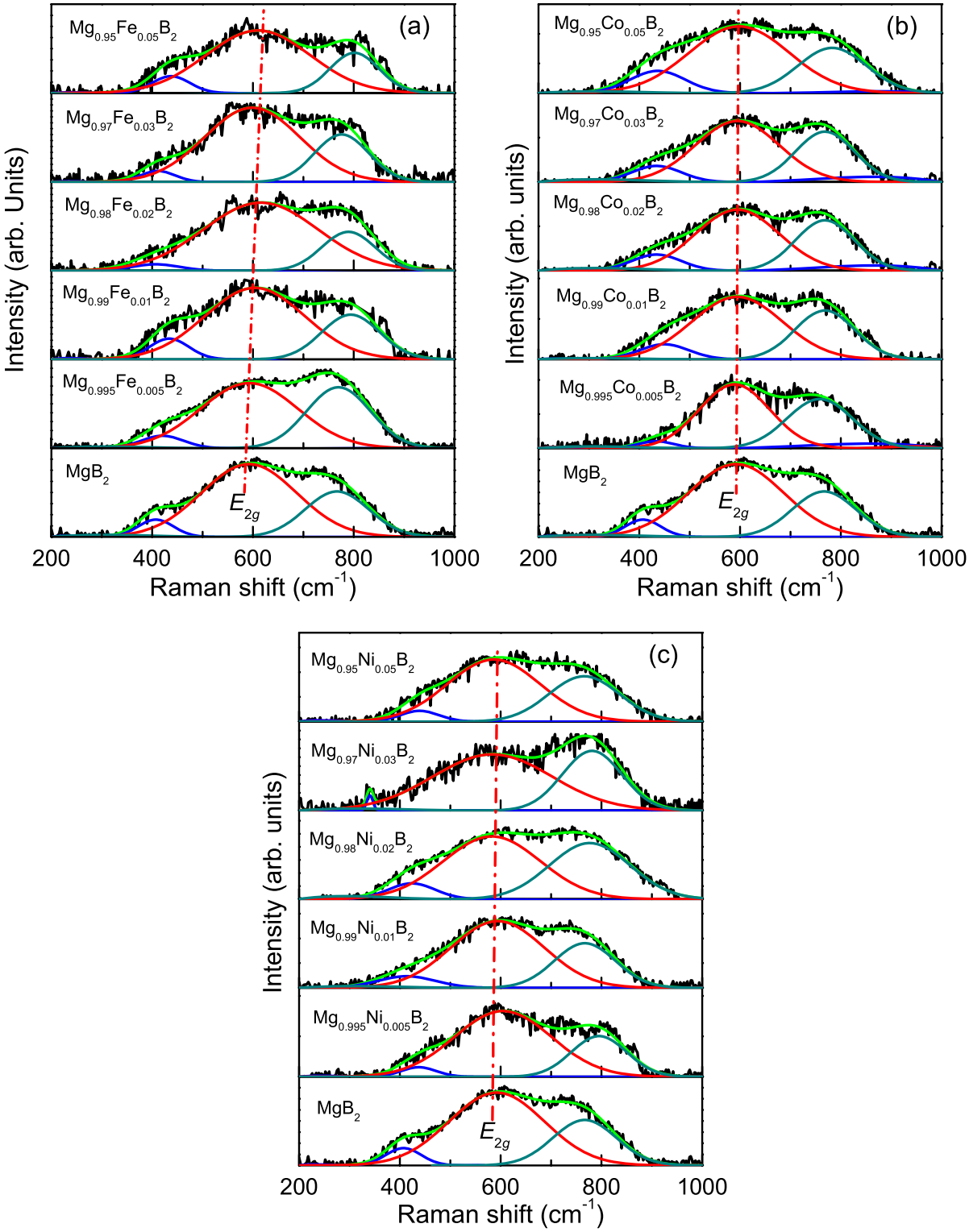

Figure 5. Raman scattering results of $Mg_{1-x}Fe_xB_2$ (a), $Mg_{1-x}Co_xB_2$ (b) and $Mg_{1-x}Ni_xB_2$ (c) fitted with three peaks. The dashed and dotted lines indicate the frequency variations of the E_{2g} mode.

surface, the only electronic property explicitly occurring in this equation. The total DOS at the Fermi level, E_F, in pure, undoped MgB_2 is $N(0) = 0.354$ states/eV cell spin, with the contribution from the σ band, $N^{\sigma}(0)$, being 0.15 and that from the π band, $N^{\pi}(0)$, being 0.204 [30]. For the Fe-doped MgB_2, the $N(0)$ values are taken for granted as constants, based on the results of nuclear magnetic resonance (NMR) measurements [6]. The $N(0)$ values of Co- and Ni-doped MgB_2 are almost the same due to their similar behavior based on the theoretical calculations [25]. Thus, $\lambda_{e-E_{2g}}$ is estimated as shown in figure 8. The coupling constants remain stable with increasing doping level for Fe- and Ni-doped samples, which

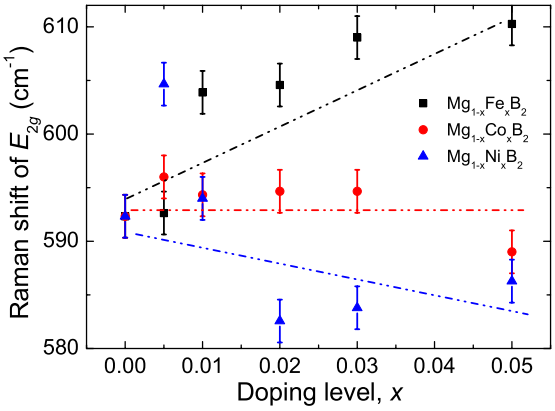

Figure 6. Fitted Raman shifts of the E_{2g} mode for $Mg_{1-x}Fe_xB_2$, $Mg_{1-x}Co_xB_2$ and $Mg_{1-x}Ni_xB_2$.

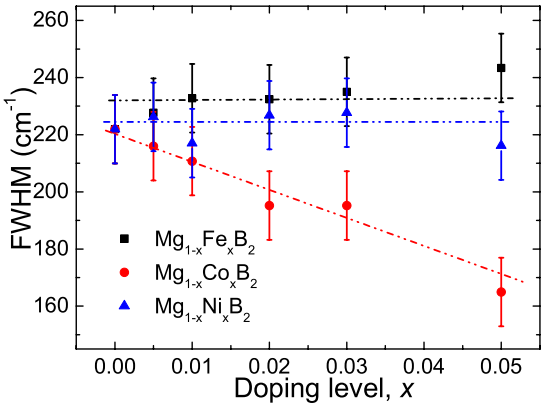

Figure 7. Fitted FWHM values of the E_{2g} mode for $Mg_{1-x}Fe_xB_2$, $Mg_{1-x}Co_xB_2$ and $Mg_{1-x}Ni_xB_2$.

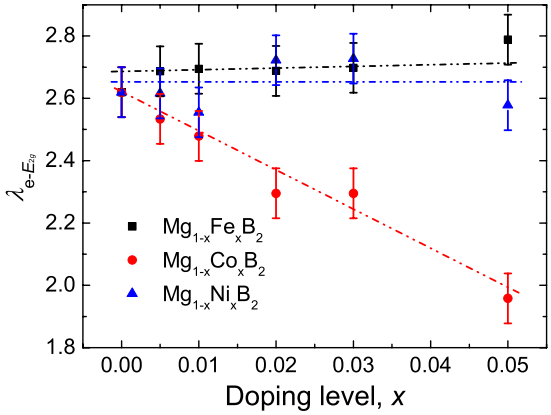

Figure 8. Estimated electron–E_{2g} coupling constants based on the fitted parameters of E_{2g} for $Mg_{1-x}Fe_xB_2$, $Mg_{1-x}Co_xB_2$ and $Mg_{1-x}Ni_xB_2$.

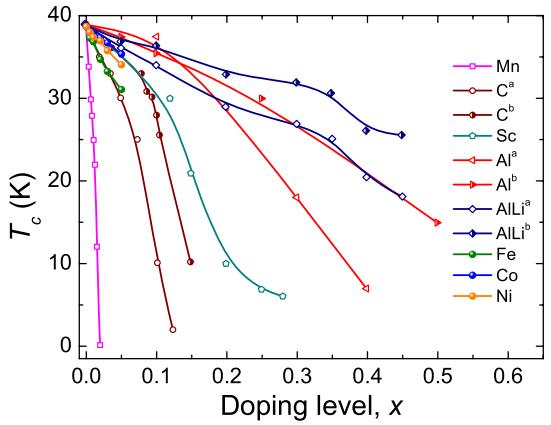

Figure 9. Comparison of T_c dependence on doping levels of Mn [4, 33], C (a from [34] and b from [35]), Al (a from [36] and b from [37]), Sc [38], AlLi ([39]: a for magnetic measurement and b for electrical measurement), Fe, Co and Ni.

means that the E_{2g} mode contribution to the superconductivity has not been weakened by the substitution effects. The results are similar to the Mn doping effects on the superconductivity of MgB_2, as shown by the unchanged Raman spectra of $Mg_{1-x}Mn_xB_2$ [31]. Considering the strong contribution of E_{2g} to the superconductivity of MgB_2, the high $\lambda_{e-E_{2g}}$ values of $Mg_{1-x}Fe_xB_2$ and $Mg_{1-x}Ni_xB_2$ are contradictory with their greatly depressed T_c. The magnetic scattering effects are responsible for the depression of the superconductivity in $Mg_{1-x}Fe_xB_2$ and $Mg_{1-x}Ni_xB_2$. The $\lambda_{e-E_{2g}}$ values of $Mg_{1-x}Co_xB_2$ drop with the increased Co contents as carbon-doped MgB_2 [32]. The decreased $\lambda_{e-E_{2g}}$ influences the total electron–phonon coupling strength of $Mg_{1-x}Co_xB_2$ and the superconductivities of $Mg_{1-x}Co_xB_2$ are strongly dependent on the characteristics of the E_{2g} mode, which is in agreement with the decreased FWHM of the E_{2g} peak.

To explore the contribution of magnetic scattering effects to the superconductivity, the dT_c/dx behaviors of $Mg_{1-x}Fe_xB_2$, $Mg_{1-x}Co_xB_2$ and $Mg_{1-x}Ni_xB_2$ are compared with those of $Mg_{1-x}Mn_xB_2$ [4, 33], $MgB_{2-x}C_x$ [34, 35], $Mg_{1-x}Al_xB_2$ [36, 37], $Mg_{1-x}Sc_xB_2$ [38] and $Mg_{1-x}(Al, Li)_xB_2$ [39], as shown in figure 9. The primary reason for the T_c decrease in Al-doped MgB_2 is likely to be the decrease in the DOS at the Fermi level by band filling and the related changes in the phonon modes, while for C doping, band scattering also has a role. However, the DOS of $Mg_{1-x}Fe_xB_2$ remains unchanged because the reduction in the DOS due to band filling effects is compensated by the increase in the DOS caused by disorder effects [6]. The Co and Ni doping influences on the DOS are also negligible from the theoretical calculations [25]. The absence of any DOS correction with Fe, Co and Ni content in MgB_2 is quite different from what occurs in $Mg_{1-x}Al_xB_2$ and $Mg(B_{1-x}C_x)_2$ [8]. As opposed to the strong magnetic pair-breaking effects in $Mg_{1-x}Mn_xB_2$, the T_c drops for $Mg_{1-x}Fe_xB_2$ and $Mg_{1-x}Ni_xB_2$ are much gentler than those of $Mg_{1-x}Mn_xB_2$ and comparable with those of the C- and Al-doped samples. This means that the magnetic scattering effects of $Mg_{1-x}Fe_xB_2$ and $Mg_{1-x}Ni_xB_2$ are too small to induce intensive pair-breaking effects via spin-flip scattering [5], which is in agreement with the weak magnetic scattering effects in the works of Joseph *et al* [2] and Lue *et al* [6]. In particular, the T_c values of low doping levels $Mg_{1-x}Fe_xB_2$ are lower than those of C-, Al- and (Al, Li)-doped samples. The magnetic scattering effect is considerable and dominant in the superconductivity when the other factors are still

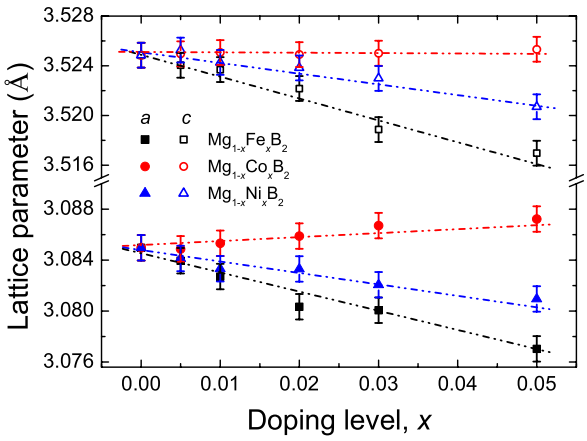

Figure 10. Refined lattice parameters of $Mg_{1-x}Fe_xB_2$, $Mg_{1-x}Co_xB_2$ and $Mg_{1-x}Ni_xB_2$ derived from the XRD patterns.

too weak to influence the superconductivity greatly because of their strong dependence on the doping concentration or substitution contents. The superconductivity of $Mg_{1-x}Ni_xB_2$ shows a similar trend and the weaker magnetic scattering effect is responsible for the higher T_c. The decreased $\lambda_{e-E_{2g}}$ value and the smaller T_c drop of $Mg_{1-x}Co_xB_2$ indicate that only the non-magnetic scattering effect is responsible for its superconductivity, which is similar to the case of Al- or Al–Li-doped MgB_2. The theoretical calculation results of Singh *et al* [34] have confirmed that Co is a magnetic dopant with a very small local moment of 0.01 μ_B in $Mg_{0.97}Co_{0.03}B_2$ and that the T_c of $Mg_{1-x}Co_xB_2$ should be lower than that of $Mg_{1-x}Fe_xB_2$ and $Mg_{1-x}Ni_xB_2$ at the same doping levels. In contrast to the theoretical calculations, rather high T_c values of $Mg_{1-x}Co_xB_2$ were obtained in our experimental results, as well as in the work of Shi *et al* [40], Kühberger *et al* [41] and Aksan *et al* [42]. Comparing the superconductivity and phonon behaviors of $Mg_{1-x}Fe_xB_2$, $Mg_{1-x}Ni_xB_2$ and $Mg_{1-x}Co_xB_2$, Fe shows the strongest magnetic moment in MgB_2 and Co the weakest.

Either disorder or chemical pressure effects due to chemical substitution are responsible for the phonon behavior [43, 44]. The lattice parameters have been refined for all the samples, as shown in figure 10. Both the *a*- and *c*-axis lattice parameters of $Mg_{1-x}Fe_xB_2$ and $Mg_{1-x}Ni_xB_2$ show obvious decreases with increasing dopant content, based on the XRD patterns, whereas those of the Co-doped samples remain stable. The strong dependence of the T_c depression on the doping level in $Mg_{1-x}Fe_xB_2$ is attributed to a combination of magnetic scattering and chemical pressure effects. The individual ionic characteristics of Fe, Co and Ni, such as mass, diameter, magnetic moment, electronic structure and active valence, may be responsible for their abilities to influence phonon behavior in MgB_2. In particular, the electronic structure and the ionic valence are responsible for the weak magnetic pair-breaking effect. It should be noted that the large mass of the Co ion is responsible for the decrease of λ_2 in $Mg_{1-x}Co_xB_2$, which is different from what occurs with the changed DOS in $Mg_{1-x}Al_xB_2$ and $Mg(B_{1-x}C_x)_2$. The observation of superconductivity in the two-band $La[O_{1-x}F_x]FeAs$ [45] also shows the independence of superconductivity from the magnetism of the component elements [46] and of any particular impurity.

4. Conclusion

In conclusion, weak magnetic scattering effects are partly responsible for the T_c depression in Fe- and Ni-doped MgB_2. The phonon behavior is mostly responsible for the slight decrease in the coupling strength in $Mg_{1-x}Co_xB_2$, as in the case of non-magnetic impurities. The ferromagnetic nature of Fe, Co and Ni does not induce strong pair-breaking in MgB_2 compared with Mn. The superconductivity of the two-band superconductor MgB_2 is independent of the magnetism of the individual component elements and of any particular impurity.

Acknowledgments

The authors appreciate useful discussions with Dr T Silver. The authors also thank the Australian Research Council for funding via a Discovery Project grant (DP0770205) and Hyper Tech Research Inc. for their financial support. YL thanks the China-Australia Government Special Fund for Science and Technology Cooperation (CH060072) and the International Cooperation Program of the Science & Technology Committee of Shanghai Municipality (075207036).

References

[1] Kortus J, Mazin I I, Belashchenko K D, Antropov V P and Boyer L L 2001 *Phys. Rev. Lett.* **86** 4656
[2] Joseph P J T and Singh P P 2007 *Solid State Commun.* **141** 390
[3] Gonnelli R S *et al* 2006 *Phys. Rev. Lett.* **97** 037001
[4] Rogacki K *et al* 2006 *Phys. Rev.* B **73** 174520
[5] Abrikosov A A and Gorkov L P 1961 *Sov. Phys.—JETP* **12** 1234
[6] Lue C S, Su T H, Xie B X, Chen S K, MacManus-Driscoll J L, Kuo Y K and Yang H D 2006 *Phys. Rev.* B **73** 214505
[7] Papavassiliou G, Pissas M, Karayanni M, Fardis M, Koutandos S and Prassides K 2002 *Phys. Rev.* B **66** 140514(R)
[8] Kortus J, Dolgov O V, Kremer R K and Golubov A A 2005 *Phys. Rev. Lett.* **94** 027002
[9] Gahtori B, Lal R, Agarwal S K, Kuo Y K, Sivakumar K M, Hsu J K, Lin J Y, Rao A, Chen S K and MacManus-Driscoll J L 2007 *Phys. Rev.* B **75** 184513
[10] Devereaux T P and Hackl R 2007 *Rev. Mod. Phys.* **75** 175
[11] Yildirim T *et al* 2001 *Phys. Rev. Lett.* **87** 037001
[12] Reich S, Leitus G and Felner I 2002 *J. Supercond.* **15** 109
[13] Rowell J M 2003 *Supercond. Sci. Technol.* **16** R17
[14] Mazin I I, Andersen O K, Jepsen O, Dolgov O V, Kortus J, Golubov A A, Kuz'menko A B and van der Marel D 2002 *Phys. Rev. Lett.* **89** 107002
[15] Shulga S V, Drechsler S L, Fuchs G, Muller K H, Winzer K, Heinecke M and Krug K 1998 *Phys. Rev. Lett.* **80** 1730
[16] Adrian S D, Wolf S A, Dolgov O V, Shulga S and Kresin V Z 1997 *Phys. Rev.* B **56** 7878
[17] Kresin V Z and Wolf S A 1992 *Phys. Rev.* B **46** 6458
[18] Kresin V Z and Wolf S A 1995 *Phys. Rev.* B **51** 1229
[19] Eliashberg G M 1963 *Sov. Phys.—JETP* **3** 696
[20] Carbotte J P 1990 *Rev. Mod. Phys.* **62** 1028
[21] Leavens C R and Talbot E 1983 *Phys. Rev.* B **28** 1304

[22] Allen P B and Mitrovich B 1982 Theory of superconducting T_c *Solid State Physics* vol 37, ed H Ehrenreich, F Seitz and D Turnbull (New York: Academic)
[23] Brinkman A, Golubov A A, Rogalla H, Dolgov O V, Kortus J, Kong Y, Jepsen O and Andersen O K 2002 *Phys. Rev.* B **65** 180517(R)
[24] Choi H J, Roundy D, Sun H, Cohen M L and Louie S G 2002 *Nature* **418** 758
[25] Singh P P and Joseph P J T 2002 *J. Phys.: Condens. Matter* **14** 12441
[26] Li W X, Li Y, Chen R H, Zeng R, Zhu M Y, Jin H M and Dou S X 2008 *J. Phys.: Condens. Matter* **20** 255235
[27] Chen X J, Zhang H and Habermeier H U 2002 *Phys. Rev.* B **65** 144514
[28] Shukla A *et al* 2003 *Phys. Rev. Lett.* **90** 095506
[29] Allen P B 1972 *Phys. Rev.* B **6** 2577
[30] Mazin I I and Antropov V P 2003 *Physica* C **385** 49
[31] Maui T, Suemitsu N, Mikasa Y, Lee S and Tajima S 2008 *J. Phys. Soc. Japan* **77** 074720
[32] Sakuntala T, Bharathi A, Deb S K, Gayathri N, Sundar C S and Hariharan Y 2005 *J. Phys.: Condens. Matter* **17** 3285
[33] Suemitsu N, Masui T, Lee S and Tajima S 2006 *Physica* C **445–448** 39
[34] Masui T, Lee S and Tajima S 2004 *Phys. Rev.* B **70** 024504
[35] Kazakov S M, Puzniak R, Rogacki K, Mironov A V, Zhigadlo N D, Jun J, Soltmann C, Batlogg B and Karpinski J 2005 *Phys. Rev.* B **71** 024533
[36] Xu G J, Grivel J C, Abrahamsen A B, Chen X P and Andersen N H 2003 *Physica* C **399** 8
[37] Renker B, Bohnen K B, Heid R, Ernst D, Schober H, Koza M, Adelmann P, Schweiss P and Wolf T 2002 *Phys. Rev. Lett.* **88** 067001
[38] Agrestini S *et al* 2004 *Phys. Rev.* B **70** 134514
[39] Monni M *et al* 2006 *Phys. Rev.* B **73** 214508
[40] Shi L, Zhang S M and Zhang H R 2008 *Solid State Commun.* **147** 27
[41] Kühberger M and Gritzner G 2002 *Physica* C **370** 39
[42] Aksan M A, Yakinci M E and Guldeste A 2006 *J. Alloys Compounds* **424** 33
[43] Li W X, Li Y, Chen R H, Zeng R, Dou S X, Zhu M Y and Jin H M 2008 *Phys. Rev.* B **77** 094517
[44] Yates K A, Burnell G, Stelmashenko N A, Kang D J, Lee H N, Oh B and Blamire M G 2003 *Phys. Rev.* B **68** 220512(R)
[45] Hunte F, Jaroszynski J, Gurevich A, Larbalestier D C, Jin R, Sefat A S, McGuire M A, Sales B C, Christen D K and Mandrus D 2008 *Nature* **453** 903
[46] Singh D J and Du M H 2008 *Phys. Rev. Lett.* **100** 237003